A Neural Anthropometer Learning from Body Dimensions Computed on Human 3D Meshes

Yansel González Tejeda
Computer Science Department
Paris Lodron University of Salzburg
Austria
https://orcid.org/0000-0003-1002-3815

Helmut A. Mayer
Computer Science Department
Paris Lodron University of Salzburg
Austria
https://orcid.org/0000-0002-2428-0962

arXiv:2110.04064v1 [cs.CV] 6 Oct 2021

***Abstract*—Human shape estimation has become increasingly important both theoretically and practically, for instance, in 3D mesh estimation, distance garment production and computational forensics, to mention just a few examples. As a further specialization, *Human Body Dimensions Estimation* (HBDE) focuses on estimating human body measurements like shoulder width or chest circumference from images or 3D meshes usually using supervised learning approaches. The main obstacle in this context is the data scarcity problem, as collecting this ground truth requires expensive and difficult procedures. This obstacle can be overcome by obtaining realistic human measurements from 3D human meshes. However, a) there are no well established methods to calculate HBDs from 3D meshes and b) there are no benchmarks to fairly compare results on the HBDE task. Our contribution is twofold. On the one hand, we present a method to calculate right and left arm length, shoulder width, and inseam (crotch height) from 3D meshes with focus on potential medical, virtual try-on and distance tailoring applications. On the other hand, we use four additional body dimensions calculated using recently published methods to assemble a set of eight body dimensions which we use as a supervision signal to our Neural Anthropometer: a convolutional neural network capable of estimating these dimensions. To assess the estimation, we train the Neural Anthropometer with synthetic images of 3D meshes, from which we calculated the HBDs and observed that the network's overall mean estimate error is 20.89 mm (relative error of 2.84%). The results we present are fully reproducible and establish a fair baseline for research on the task of HBDE, therefore enabling the community with a valuable method.**

***Index Terms*—Human Body Dimensions Estimation, Deep Learning, Human Shape Estimation**

I. Introduction

Human shape analysis has been, historically, an active area of research. Recently, as a further specialization, *human shape estimation* (HSE) has been established as a solid scientific field whose main concern is to investigate methods to infer the shape of a human body from underconstrained information.

Depending on these methods' input, HSE scenarios can be categorized as estimation from imagery (2D) or point clouds or meshes (3D). Regarding the output, there are two tasks commonly performed, namely a) parameter estimation, e.g., estimation of SMPL (Skinned Multi-Person Linear) model parameters; and b) estimation of a surface that best explain the input image, a.k.a. 3D reconstruction, or more recently, human mesh recovery.

However, the task of human body dimensions estimation (HBDE) has, to date, received significantly less attention. Human body dimension (HBD) refers in this context to anthropometrical measurements, e.g., shoulder width or crotch height. Predicting these 3D human body measurements from images is fundamental in several scenarios like virtual try-on, animating, ergonomics, computational forensics and even health and mortality estimation [2].

The HBDE problem given a single image is an inverse (underconstrained) problem. If we consider the human body dimensions as the 'cause' and the images of these humans as the observations, then our goal is to calculate from a set of observations the causal factors. Furthermore, information gets lost when a camera is used to capture the human body in 3D space to form a 2D image. This problem may be tackled by a supervised learning approach, specifically, convolutional neural networks (CNNs). The fundamental challenge of this approach is to overcome the data scarcity problem. A moment of thought reveals the extraordinary effort demanded by the collection of these data: thousands of people would have to be measured and photographed. While such a survey has been conducted in the past (CAESAR project [3]), we need to investigate different approaches that are not confronted with this heavy burden. Accordingly, we explore an alternative method where HBDs are not derived from real people, but from models of real humans.

Generating 3D realistic human bodies and performing anthropometrical measurements on them is by no means a trivial task. Despite practitioners having a general idea, there is no consens regarding how each of these measurements (if any) should be measured, neither in 3D models nor even in humans. Moreover, in the rare case that the procedure to measure a particular HBD is well established among anthropometrists and tailors, it often refers to human body landmarks (HBL) and anatomical joints (AJ). For example, the European clothing standard EN 13402 defines arm length as "distance, measured using the tape measure, from the armscye/shoulder line intersection (acromion), over the elbow, to the far end of the prominent wrist bone (ulna), with the subject's right fist clenched and placed on the hip, and with the arm bent at 90°". These points of reference (HBL and AJ) pose a challenging scenario for computer vision systems. On the one side HBL

©2021 IEEE. Personal use of this material is permitted. Permission from IEEE must be obtained for all other uses, in any current or future media, including reprinting/republishing this material for advertising or promotional purposes, creating new collective works, for resale or redistribution to servers or lists, or reuse of any copyrighted component of this work in other works.

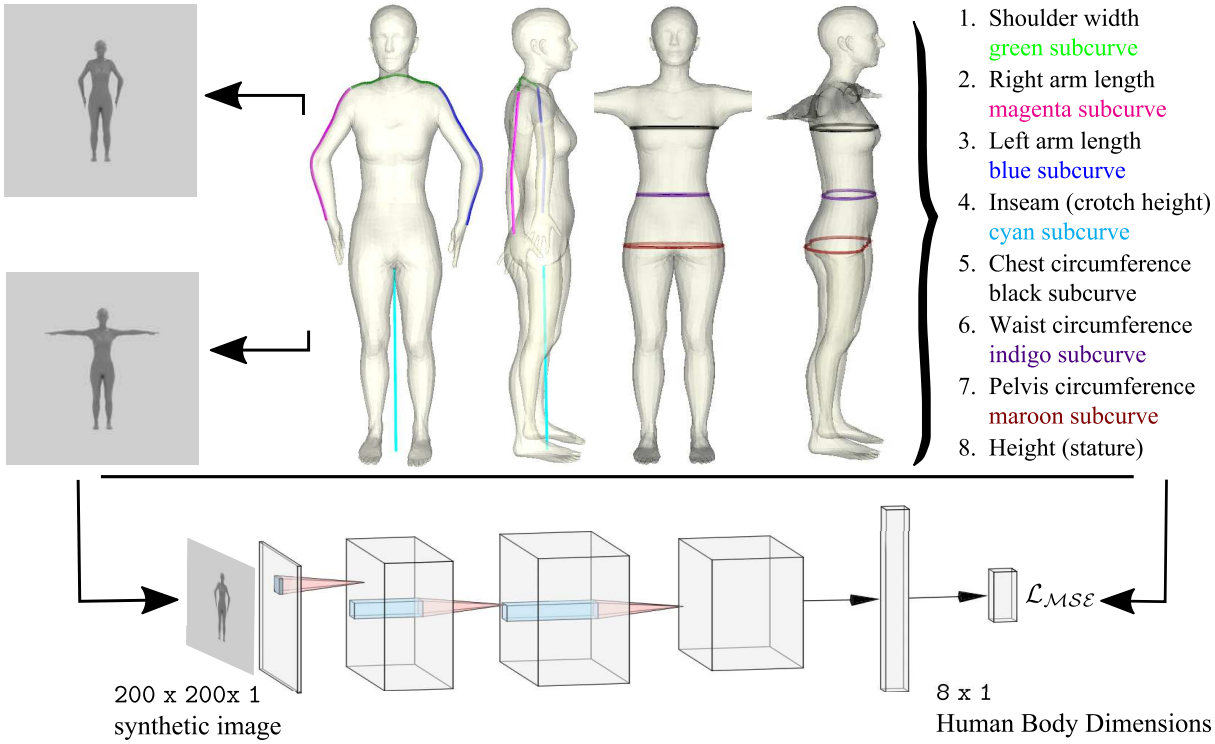


Fig. 1. The Neural Anthropometer framework: a CNN that is able to estimate human body dimensions from synthetic images of persons in two poses. We propose to address the problem of data scarcity in estimating human body dimensions by establishing methods to compute them from 3D meshes. Top center: we present a method to calculate shoulder width, right and left arm length and inseam (crotch height). In addition to these human dimensions, we use Calvis [1] to augment the set with four more measurements plus height (top right). We then synthesize grayscale 200 pixels square images (200 x 200 x 1) from 3D female and male (not shown) meshes in two poses to use them as input to a CNN (top left). Bottom: The Neural Anthropometer can be fed with these synthetic images. The supervision signal is a vector of eight human body dimensions and the loss is the Mean Square Error $\mathcal{L}_{MSE}$ between the actual and the estimated measurements. The network architecture is described in subsection III-D.

are not well defined and on the other side AJ are not visible.

Yet another problem is the comparability of results related to HBDE. Since the methods to compute HBDs are not consistent, the estimation results can not be fairly compared. For example, [4] examined four garment pattern preparing systems and found that HBDs differed entirely among them and all violated anthropometric rules. We are keen to advance the field in this matter by making our method's implementation publicly available.

Let us turn now to the problem of HBDE.

A. The Problem of Estimating Human Body Dimensions

Our goal is, given an image $\mathcal{I}$ from a 3D human body with HBD D, to return a set of estimated human body dimensions. Let us denote the estimated dimensions vector as $\hat{D}$, then our problem is to train a CNN $\mathcal{M}$ that has a good generalization performance such that (at least approximately)

$$\hat{D} = \mathcal{M}(\mathcal{I}(D)) \tag{1}$$

Elements of the human dimensions vector D are, in general, body measurements like height, shoulder width, and waist circumference, or other shape information like body surface area, weight, or body fat percentage, to mention just a few examples. The elements of $\hat{D}$ are their estimated values. In this paper, we focus on eight of these human body dimensions, namely, shoulder width, right and left arm length and inseam (crotch height); chest, waist and pelvis circumference and height (stature).

We assume that we draw the dataset from the generating distribution $\mathcal{G}$. The model $\mathcal{M}$ minimizes the probability, $C(\mathcal{M})$, of making a wrong prediction:

$$C(\mathcal{M}) = \Pr_{(\mathcal{I},D)\sim\mathcal{G}}[\mathcal{M}(\mathcal{I}) \neq D] \tag{2}$$

Note that this is a deep regression (in contrast to a classification) multitask learning problem [5]. The term deep regression has become popular over the past few years in the context of deep learning. However, the lack of its systematic evaluation has been recently criticized [6].

B. Contributions and scope

Our key contribution is the Neural Anthropometer approach: a method to obtain eight HBDs from 3D human meshes that we use as a supervision signal to conduct HBDE with a CNN whose inputs are synthetic images from those meshes (Fig. 1).

We believe that our fully reproducible method to obtain ground truth provides the scientific community with a valuable methodology for HSE in general and particularly for

HBDE. Moreover, the Neural Anthropometer estimation results establish a solid baseline that researchers can use to compare future work to. Upon publication, we will make our code publicly available for research purposes under https://github.com/neoglez/neural-anthropometer.

In this paper, we will first review briefly the state of art, as well as our approach to compute human body dimensions from 3D models and use them for supervised learning. We will then present one experiment that illustrates the plausibility of our approach. Finally, we will discuss important aspects of our findings.

II. Related Work

In this section we present research relevant to our goal. We group related work around topics of interest in HSE.

A. Human Body Dimensions Estimation from Images.

Previous research has used HBDs directly recovered from individuals to estimate body measurements from images [7], [8]. Height, arm span and even weight have been employed as ground truth. Chest and waist size have been considered as well [9]. In contrast, we do not conduct measurements directly on humans, but calculate them consistently from 3D meshes. Other researches focus on an small set of dimensions or even only one. For example, [10] estimates height in surveillance areas. A set of three HBDs (chest, waist and pelvis circumference) is defined by [1]. We augment this set with four more dimensions.

Another significant research direction studies shape as parameters of some model. For example [11] claim describing the first method to estimate pose and shape from a single image, while [12] estimates shape from 91 keypoints using decision forests. Shape is understood as SMPL model [13] parameters but not human dimensions. In general, previous work has concentrated in parameter or 3D mesh estimation (mesh recovery). In contrast, we focus in estimating human body measurements in an end-to-end manner.

B. Human Body Data Synthesis.

The Shape Completion and Animation of People (SCAPE) model [14] opened wide possibilities in the field of human shape estimation. It provided the scientific community with a method to build realistic 3D human body meshes of different shapes in different poses. In order to synthesize a human body mesh a template body must be deformed. The model exhibits, however, an important limitation, namely the last step on the pipeline is an expensive optimization problem. Other researchers had used variation of the SCAPE model (S-SCAPE [15]) to synthesize human bodies but focused on people detection. After some attempts on improving the human models quality, for example, to make more easily capturing the correlation between body shape and pose [16], or to better understand body dimensions (Semantic Parametric Reshaping of Human Body Models - SPRING model [17]), Loper et al., 2015 [13] developed the SMPL generative human body model. In subsection III-A we synthesize 3D human meshes using this model. Our approach to synthesize images from 3D meshes has been influenced by the recent publication of the large scale dataset SURREAL [18]. This work uses the SMPL model to generate images from humans with random backgrounds. However, no human body dimensions are computed or estimated.

More recently, other models have been presented: [19] introduced a human model with added hands and face and [20] propose STAR, which is trained on a dataset of 14,000 human subjects. We do not use these more complex models because the human dimensions we estimate do not require such level of detail.

C. Digital Anthropometry on 3D Models.

Although extensive research has been carried out on human shape estimation, methods to consistently define shape based on 3D mesh anthropometric measurements have been little explored. Only a handful of researchers have reported calculating 1D body dimensions from 3D triangular meshes to use them as ground truth for training and validation in a variety of inference processes.

Early research performed feature analysis on what they call body intuitive controls, e.g. height, weight, age and gender [21] but they do not calculate them. Instead they use the CAESAR demographic data. Recording human dimensions beyond height like body fat and the more abstract “muscles” are described by [16].

Pertinent to our investigation is also the inverse problem: generating 3D human shapes from traditional anthropometric measurements [22]. Like this work we use a set of anthropometric measurements that we call dimensions, unlike them we calculate 1D measurements from 3D human bodies to use them as ground truth for later inference.

Strongly related to our work are methods that calculate waist and chest circumference by slicing the mesh on a fixed plane and compute the convex hull of the contour [9] or path length from identified (marked) vertices on the 3D mesh [23]–[26]. However, is not clear how they define the human body dimensions.

In contrast, we do not calculate the dimensions from fix vertices on the template mesh. Instead, we adopt a more anthropometric approach and use domain knowledge to calculate these measurements.

D. Human Shape Estimation with Artificial Neural Networks

A huge amount of research has been conducted in recent years to address the problem of 3D/2D human shape estimation using CNNs. State-of-the-art methods are [27]–[29] where they estimate human shape and pose (recently with evolutionary techniques [30]) or directly regress 3D vertex coordinates [31]. While these CNN’s output are human body models parameters (i.e., βs in [24] and [32]) or 3D human pose (i.e., 3D human key-point coordinates) or both [33] our network is capable to output human dimensions directly, enabling new perspectives in HSE.

III. Approach

In order to train our neural anthropometer with images of humans and be able to use human body dimensions as ground truth, we base our approach on three main aspects: a) 3D human mesh synthesis with the SMPL model [20], b) calculation of human body dimensions and c) 2D image synthesis of the generated meshes. While a) and c) have been treated and employed by previous work, our fundamental contribution lies in b) and the CNN that we train to conduct HBDE. We now turn to discuss these aspects.

A. 3D human mesh synthesis with SMPL model

Basically, we use SMPL as generative model because it is derived from real humans. This feature guarantees, to a large extent, the 3D mesh level of realism and, correspondingly, the correctness of the human body dimensions we calculate. Thereof, SMPL has been widely adopted by researchers and industry and is the model of preference in HSE.

The SMPL model contains a template mesh (mean template shape $\bar{\mathbf{T}}$ in the zero pose $\vec{\theta^*}$) that can be deformed according to shape parameters $\vec{\beta}$. Both template and the 3D models resulting from synthesis have a mesh resolution of $N = 6890$ vertices. Additionally, SMPL attaches a skeleton to the template mesh. The 3D model can then be posed according to pose parameters $\vec{\theta}$. This feature plays an important role in our methodology since HBDs are commonly defined based on skeleton joints. The skeleton $\mathbf{J}$ is defined by its joints location in 3D space $j_i \in \mathbb{R}^3$ and its kinematic tree. Two connected joints define a "bone". Moreover, a child bone is rotated relative to its connected parent. The pose description $\vec{\theta}$ is the specification of every bone rotation plus an orientation for the root bone.

When synthesizing the human meshes, we aim at gaining high variability of human bodies. However, how to choose shape parameters $\vec{\beta}$ *such as the variability in the data is as high as possible* is not trivial. If the shape parameters are not carefully chosen, either the human meshes look notably similar or so called monster shapes might be generated. Understandably, we want to avoid such monster shapes, even at the cost of sacrificing variability. Other researchers have avoided this problem by fitting the SMPL model to already existing 3D meshes [18]. But this implies collecting the 3D meshes in the first place and performing expensive optimizations. We circumvent this phase by uniformly varying shape parameters from -3 to 3 standard deviations.

Beside shape, we have to consider pose $\vec{\theta}$ as well, as for a number of HBDs (in real life) a person is asked to adopt a pose other than the zero pose $\vec{\theta^*}$. Intuitively, to compute our HBDs, we would like to mimic the procedure conducted by a tailor or anthropometrist. Although these two procedures differ slightly, for the measurements we investigate, the subject must lower her arms (shoulders need to hang naturally in a relaxed position). However, we observe that if we impose this in general for all 3D scans, and due to the fact that we are working with Linear Blend Skinning (which produces artifacts) inter-penetrations occur. Therefore, we bend the arms (set both shoulder rotation) by 30 degrees and elbows by 18.75 degrees. Following the convention that the template mesh is in the zero pose $\vec{\theta^*}$, we define this new pose as **pose 1** ($\vec{\theta^1}$), see Fig. 2.

We then synthesize 6000 female and 6000 male 3D meshes in poses $\vec{\theta^*}, \vec{\theta^1}$ and proceed with the HBDs' calculation.

B. Computation of HBDs

Regarding our HBDs' calculation, our general approach is to use ray casting originating in skeleton joints to establish landmarks on the 3D mesh. All of our landmarks arise as a result of a cast ray intersecting the mesh in a specific point. In fact, these landmarks allows us to perform length computations. For example, the length of a subcurve that connects specific landmarks. Nonetheless, length queries and curve fitting methods on manifolds are in general, and specifically on 3D shapes, highly complex. Therefore, we pursue solutions that while simulating the way measurements are taken in real life, simultaneously are as efficient as possible.

Using landmarks and bounding box associated points, we define planes to intersect the mesh. The result of an intersection may be a collection of curves both open and closed. Let us restrict our attention to closed curves that possibly contain two landmarks. These landmarks separate the closed curve in two subcurves. We can then make certain assumptions and associate the length of a subcurve with the desired HBD. We now define all required landmarks (see Fig. 3) to explain HBD computation bellow.

- u_{rs} and u_{ls} generated by the mesh intersection of a ray from right and left **shoulder joints**, in direction perpendicular to the rear edge of the bounding box's top face, respectively.
- u_{re} and u_{le} generated by the mesh intersection of a ray from right and left **elbow joints**, in direction perpendicular to the right and left bounding box's face, respectively.
- u_{rw} and u_{lw} generated by the mesh intersection of a ray from right and left **wrist joints**, in direction perpendicular to the right and left bounding box's face, respectively.
- u_{ch} generated by the mesh intersection of a ray with the **pelvis joint** in direction perpendicular to the floor (bounding box's bottom face).

Additionally, we calculate subject height h (stature), without further elaboration, as the bounding box's height.

1) Shoulder width: For this body dimension, we use landmarks u_{rs} and u_{ls} defined above, see Fig. 2. Intuitively, we would extend a virtual tape over the mesh surface (skin) to measure the length of a path joining these two points. In order to complete the solution, we must further constraint the path to live in a subcurve resulting from a plane π_{sw} containing the landmarks.

To construct the plane three non-colinear points must be defined; landmarks u_{rs} and u_{ls} are two of them. However, we need a third point p_c. A key insight is that plane π_{sw} should not be parallel to any of the bounding box's faces, as the generated curve would be either too low or two high in the back of the subject. Therefore, after some experiments we came up with

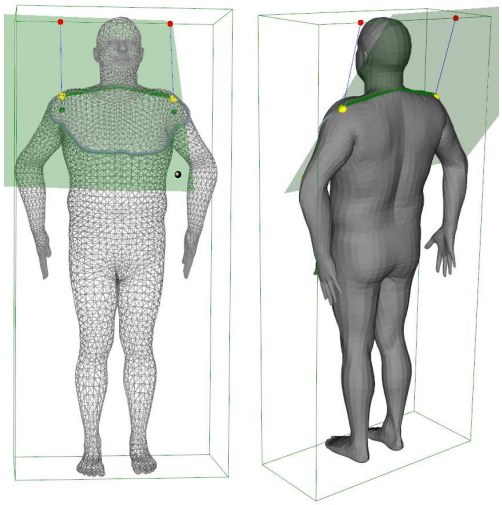


Fig. 2. Shoulder width calculation. The 3D (male) mesh is in **pose one** $\vec{\theta^1}$. Green spheres inside the mesh are skeleton joints. Yellow spheres are skin landmarks (here u_{rs} and u_{ls}) determined by casting a ray from the corresponding skeleton joint perpendicular to the bounding box. Red spheres are ray intersection points with the bounding box. The point p_c is the black sphere (slightly translated for visualization purposes). The plane π_{sw} (light green) defined by u_{rs}, u_{ls} and p_c cuts the mesh and delimits a boundary curve. On the left side we show the subject frontal view, where the boundary curve can be seen. On the right side, landmarks u_{rs} and u_{ls} can be used to further split the curve in two subcurves. We assume that the least length subcurve is the shoulder width (green bold subcurve). The resulting shoulder width for this male subject ($height = 181.11\,cm$) is $47.60\,cm$

a heuristically determined point p_c. The y-coordinate is set to be 65% of the height, the x-coordinate refers to the symmetry axis of the body (middle), and the z-coordinate is given by the maximal z-value of the complete mesh ("thickest point"). As a consequence, we get a plane, which is adapted to the body shape.

We slice the mesh with π_{sw} and obtain the boundary curve. We merely have to decide which of the subcurves corresponds to the shoulder width. We do that by computing the path length of the two subcurves and assuming the shoulder width to be the shorter path length.

2) Arm length (sleeve length): Similarly to how we calculate shoulder width, we proceed with arm length calculation. In this subsection, we describe the method for right arm length. The left arm length calculation is handle using exactly the same methodology, albeit with corresponding landmarks (see Fig. 3).

For this dimension we use landmarks u_{rs}, u_{re}, and u_{rw}. A plane π_{ral} defined by these three points cuts the mesh and yields a number of polygonal curves (possibly open and closed). We observe that this step produces frequently more than a single curve. Therefore, we are forced to explicitly search for the right curve containing the landmarks.

Theoretically, this search should not pose further complications. In practice, floating point operations are an important issue due to their limited precision. Thus, we introduce a tolerance parameter $tol = 0.001$ and deem a point to be found when it is within the tolerance.

Once we find the desired curve, we proceed in the same manner as for the shoulder width calculation: we use u_{rs} and u_{rw} to extract two subcurves. We then can consider the right arm length to be the subcurve with minimum x coordinate and calculate its length.

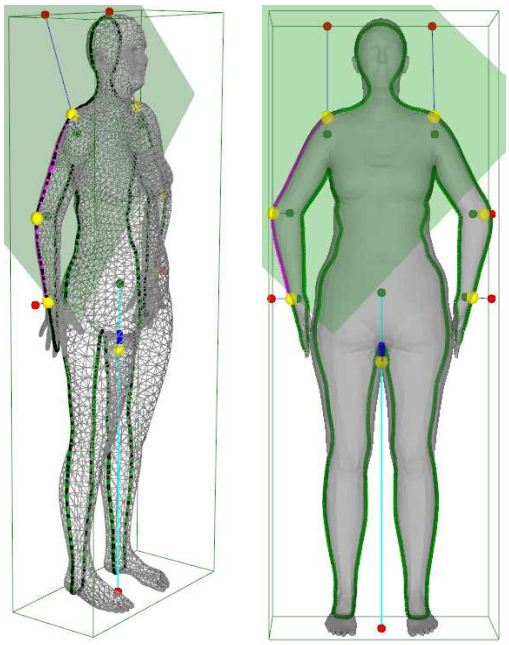


Fig. 3. Right arm length (magenta subcurve) and inseam length (cyan line) calculation. Green, yellow and red spheres representation is as described in Fig. 2. Following landmarks are shown: from subject's view, starting at the crotch region, clockwise: u_{ch}, u_{lw}, u_{le}, u_{ls}, u_{rs}, u_{re} and u_{rw}. The light green plane defined by three of the corresponding same side landmarks (shoulder, elbow and wrist) cuts the mesh and defines a boundary curve. Left: intersection points of the plane with mesh triangles (edge or face) are shown in black. Right: subject frontal view. Two skin landmarks (here u_{rw} and u_{rs}) can be used to further split the curve in two subcurves. We assume that the subcurve being proxy to the corresponding arm length has minimum x coordinate (right), respectively, maximum x coordinate (left). To compute the inseam, we cast a ray in direction to the floor. Note that this ray might intersect the mesh in more than one point (shown in blue). We define the inseam as the length from the last point of this set (u_{ch}) to the floor. The resulting right arm and inseam length for this female subject ($height = 196.05\,cm$) are $64.67\,cm$ and $85.72\,cm$, respectively.

Not surprisingly, this method does not yield equal right and left arm length. Curiously, despite our computations being conducted on 3D meshes, this type of asymmetry is also observed in modern humans [34].

3) Inseam: The inseam is informally defined as the length of the shortest path between the crotch (perineum) and the floor. Therefore, we calculate the euclidean distance from landmark u_{ch} to the bounding box's bottom face, see Fig. 3.

At this point, we have calculated our four HBDs. Since Calvis use the SMPL model as well, we are able to easily calculate the other three HBDs, therefore, completing our formulation.

C. 2D image synthesis for network input

After having calculated the HBDs, we continue with the synthesis of the neural anthropometer's input: 2D images of the 3D meshes.

For the synthesis we use the Blender package [35], adapting the method described in previous work [1], [18]. Specifically, we employ Cycles rendering engine with an orthographic camera model. The orthographic camera has a resolution of 200×200, focal length of $60\,mm$, sensor size of $32\,mm$ and orthographic scale of 2.5. We keep fix the camera at a distance of $6\,m$ in front of the mesh and produced a grayscale image.

Having synthesized input and supervision signal, we are now ready to detail the neural anthropometer architecture.

D. Neural Anthropometer Architecture

The neural anthropometer architecture is shown in Fig. 1 and we implement it with Pytorch [36]. Our intention is to keep the network as small as possible, since such a network is easier to train and consumes less resources . The input layer processes a fixed image of size `200 x 200 x 1` by applying a convolution with a 5-pixels square kernel to produce a feature map of size `196 x 196 x 8`. The intuition behind choosing the number of channels is that the network might need at least one channel per HBD in the first stage to achieve good performance. The tensor is then passed through a rectified linear unit (ReLU) [37] and batch normalization is applied. Next, max pooling with stride 2 is used before the tensor is send to a second convolutional layer with a 5-pixels square kernel and 16 output channels, resulting in a tensor of size `94 x 94 x 16`. The same pooling strategy as before is applied and the output is flatten to a tensor of size `35344`. This tensor is passed to a fully connected layer and again through a ReLU. The last layer is a regressor that outputs the eight human body dimensions in meters.

IV. Experiment and Results

We suppose that the neural anthropometer can infer the HBDs from images of humans in different poses. To better understand this phenomenon, we train and evaluate the network with all images, regardless of gender or pose, in a k-fold cross-validation setting ($k = 5$).

We conduct our experiment with the neural anthropometer on the dataset we produced. Let us briefly recapitulate its structure. The dataset comprises 12000 human body meshes from 6000 subjects generated with SMPL: 3000 female meshes in **pose 0** and 3000 in **pose 1**; equivalently, 3000 male meshes in **pose 0** and 3000 in **pose 1**. From each mesh, we synthesize a grayscale image of size `200 x 200 x 1`. Therefore, the dataset contains 12000 synthetic pictures of the subjects. Further, for each subject, we calculate a set of eight HBDs: shoulder width, right and left arm length, inseam; chest, waist and pelvis circumference and height.

For training, we randomly selected images of female and male objects in **pose 0** and **pose 1**. We train the neural anthropometer for 20 epochs and use mini-batches of size 100. We minimize **MSE** between the actual and the estimated HBDs using stockading gradient descent with momentum (Pytorch's method modified from [38]). We set learning rate to 0.01 and momentum to 0.9. We perform this experiment on a PC with Intel(R) Core(TM) i7-7700K CPU and NVIDIA GeForce GTX 1060Ti.

HBD	MAD	RPE(%)
Shoulder width	12.54	4.93
Right arm length	12.98	2.22
Left arm length	13.48	2.34
Inseam/crotch height	22.17	3.12
Chest circumference	25.22	2.51
Waist circumference	27.53	3.67
Pelvis circumference	25.85	2.40
Height	27.34	1.58
AMAD	20.89	
ARPE		2.84

TABLE I
NEURAL ANTHROPOMETER'S ESTIMATION RESULTS. DISPLAYED ARE THE MAD FOR EACH HUMAN BODY DIMENSION (FIRST COLUMN) OVER FIVE FOLDS, EXPRESSED IN MILLIMETERS (SECOND COLUMN). THE THIRD COLUMN SHOWS THE RPE. THE LAST TWO ROWS DISPLAY AMAD AND ARPE OVER ALL HBDS AND FOLDS.

A. Quantitative Evaluation

As model evaluation we use k-fold cross validation ($k = 5$), e.g., each fold j contains $a = 2400$ instances for evaluation, from which we estimate eight HBDs using the neural anthropometer. Therefore, we report statistics based on a results tensor of shape

$$k \times a \times |\{\hat{D}_i, D_i\}| \times 8 = \texttt{5 x 2400 x 2 x 8}. \tag{3}$$

We report estimation error e^i_{MAD} for each HBD i as the Mean Absolute Difference over the j folds between estimated and actual HBDs $\hat{D}_i$, D_i, respectively:

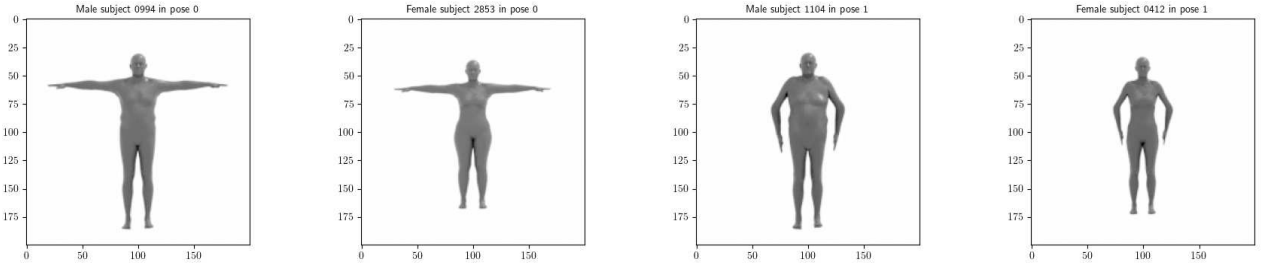
$$e^j_{MAD} = \frac{1}{a}\sum_{l=1}^{a}|\hat{D}_l - D_l|, \quad e^i_{MAD} = \frac{1}{k}\sum_{j=1}^{k} e^j_{MAD} \tag{4}$$

Additionally, we find helpful to consider Relative Percentage Error (RPE) e^i_{RPE} for each HBD i and its Average (ARPE);

$$e^j_{RPE} = \frac{1}{a}\sum_{l=1}^{a}|\frac{\hat{D}_l - D_l}{D_l}|, \quad e^i_{RPE} = \frac{1}{k}\sum_{j=1}^{k} e^j_{RPE} \tag{5}$$

Like prior research, we report Average Mean Absolute Difference (AMAD) over the eight HBDs $e_{AMAD} = \frac{1}{8}\sum_{j=1}^{8} e^i_{MAD}$.

Results are shown in Table I. From the table, it can be seen that the prediction of shoulder width exhibits the highest relative estimation error (4.93%), while height prediction manifests lowest relative error (1.58%). Interestingly, right and left arm length prediction error (2.22% and 2.34%, respectively) are closest to each other than to any other estimation error. Overall, the neural anthropometer is able to predict the HBDs with average relative error of 2.84%.



HBD	Actual	Predicted	Error (%)
CC	122.25	124.10	+1.52
H	193.99	193.31	-0.35
I	90.27	88.95	-1.46
LAL	65.79	64.63	-1.76
PC	114.60	114.89	+0.25
RAL	65.95	65.82	-0.19
SW	48.33	47.06	-2.64
WC	112.82	112.26	+1.52

HBD	Actual	Predicted	Error (%)
CC	99.61	100.76	+1.16
H	164.59	164.31	-0.17
I	67.86	68.90	+1.53
LAL	58.94	58.05	-1.50
PC	114.25	112.28	-1.72
RAL	59.16	58.43	-1.23
SW	36.25	37.12	+2.41
WC	86.91	86.20	+1.16

HBD	Actual	Predicted	Error (%)
CC	134.40	132.56	-1.37
H	195.12	195.36	+0.12
I	88.61	88.36	-0.28
LAL	65.17	66.67	+2.29
PC	119.96	118.38	-1.32
RAL	67.30	66.71	-0.88
SW	46.49	46.69	+0.44
WC	120.46	121.82	-1.37

HBD	Actual	Predicted	Error (%)
CC	93.08	94.11	+1.10
H	174.23	174.42	+0.10
I	75.02	77.11	+2.79
LAL	59.62	57.72	-3.18
PC	98.04	97.73	-0.31
RAL	58.31	57.18	-1.93
SW	36.17	36.10	-0.18
WC	79.17	78.84	+1.10

Fig. 4. Estimation results on four selected subjects, two female and two male. Abbreviations are as follows. CC: chest circumference, H: height, I: inseam, LAL: left arm length, PC: pelvis circumference, RAL: right arm length, SW: shoulder width, WC: waist circumference.

B. Visualization and Discussion

Let us visualize a four instances mini-batch. We select randomly one of k models saved during training to make inference. Fig 4 shows human body dimensions estimation of four selected subjects.

Fig 4 is quite revealing in several ways. First, consider the first two subjects (male subject 0994 and female subject 2853). Both subjects are in pose 0 and their shoulder width prediction error (-2.64% and 2.41%) is higher than the other two (in pose 1). This may indicate that for network is not easy to predict shoulder width when the person is in pose 0. Secondly, as it might be expected, height exhibits across all subjects and HBDs the lowest error (-0.35%, -0.17%, $+0.12\%$ and $+0.10\%$). This result has further strengthened our confidence in considering the height as the less difficult predictable HBD. Finally, while the right and left arm length is mostly underestimated, the error is slightly higher in the case of left arm length.

We believe that it might not be reasonable to improve some of the results we present here. For example, the difference between estimated and actual height is in the order of mm. That means that estimation is already being performed at a precise level. Probably, in most scenarios, this level of sensitivity is not needed. On the other hand, it is practical to improve estimation error for other HBDs like arm length. Here, we observe that the estimation error is probably relevant for applications like distance tailoring. This suggests that, depending on the context, AMAD might not be optimal to evaluate results, since the estimation error of the HBDs are equally weighted. A weighted average could be more desirable when reporting results.

V. Conclusion

We presented the neural anthropometer, a CNN capable of estimating eight human body dimensions from synthetic pictures of humans. To obtain ground truth for training, we introduced a method to calculate four human body measurements (shoulder width, right and left arm length, and height) from 3D human meshes. We then augmented this set with four human body dimensions calculated using recently published methods. This method constitute an innovation that can be used by researchers to push the boundaries of Human Shape Estimation. We then input the images to the CNN and minimized the Mean Square Error between the estimated and the calculated human body dimensions. Our experiments revealed that the neural anthropometer is able to accurate estimate eight human body measurements with a mean absolute difference of 20.89 mm (relative error of 2.84%).

References

[1] Y. González Tejeda and H. A. Mayer, "Calvis: chest, waist and pelvis circumference from 3D human body meshes as ground truth for deep learning," 2020, 14 pages, 6 figures. To appear in the Proceedings of the VIII International Workshop on Representation, analysis and recognition of shape and motion FroM Imaging data (RFMI 2019), 11-13 December 2019, Sidi Bou Said, Tunisia. 2, 3, 6

[2] S. B. Heymsfield, B. Bourgeois, B. K. Ng, M. J. Sommer, X. Li, and J. A. Shepherd, "Digital anthropometry: a critical review," *European Journal of Clinical Nutrition*, vol. 72, no. 5, pp. 680–687, May 2018. [Online]. Available: https://doi.org/10.1038/s41430-018-0145-7 1

[3] K. M. Robinette, H. Daanen, and E. Paquet, "The caesar project: a 3-d surface anthropometry survey," in *Second International Conference on 3-D Digital Imaging and Modeling (Cat. No. PR00062)*. IEEE, 1999, pp. 380–386. 1

[4] A. S. Kilic and Z. Öndogan, "Evaluating and defining body measurements according to anthropometric measurement technique for lower garment pattern preparation." *Journal of Textile & Apparel/Tekstil ve Konfeksiyon*, vol. 26, no. 1, 2016. 2

[5] X. Zhen, M. Yu, X. He, and S. Li, "Multi-target regression via robust low-rank learning," *IEEE Trans. Pattern Anal. Mach. Intell.*, vol. 40, no. 2, pp. 497–504, 2018. [Online]. Available: https://doi.org/10.1109/TPAMI.2017.2688363 2

[6] S. Lathuilière, P. Mesejo, X. Alameda-Pineda, and R. Horaud, "A comprehensive analysis of deep regression," *CoRR*, vol. abs/1803.08450, 2018. [Online]. Available: http://arxiv.org/abs/1803.08450 2

[7] C. BenAbdelkader and Y. Yacoob, "Statistical body height estimation from a single image," in *8th IEEE International Conference on Automatic Face and Gesture Recognition (FG 2008), Amsterdam, The Netherlands, 17-19 September 2008*, 2008, pp. 1–7. [Online]. Available: https://doi.org/10.1109/AFGR.2008.4813453 3

[8] L. Sigal, A. Balan, and M. J. Black, "Combined discriminative and generative articulated pose and non-rigid shape estimation," in *Advances in Neural Information Processing Systems 20*, J. C. Platt, D. Koller, Y. Singer, and S. T. Roweis, Eds. Curran Associates, Inc, 2008, pp. 1337–1344. [Online]. Available: http://papers.nips.cc/paper/3271-combined-discriminative-and-generative-articulated-pose-and-non-rigid-shape-estimation.pdf 3

[9] P. Guan, "Virtual human bodies with clothing and hair: From images to animation," Ph.D. dissertation, Department of Computer Science at Brown University, 2013. [Online]. Available: http://cs.brown.edu/pguan/publications/thesis.pdf 3

[10] K. V. Sriharsha and P. J. A. Alphonse, "Anthropometric based real height estimation using multi layer peceptron ann architecture in surveillance areas," in *2019 10th International Conference on Computing, Communication and Networking Technologies (ICCCNT)*, 2019, pp. 1–6. 3

[11] F. Bogo, A. Kanazawa, C. Lassner, P. Gehler, J. Romero, and M. J. Black, "Keep it SMPL: Automatic estimation of 3D human pose and shape from a single image," in *Computer Vision – ECCV 2016*, ser. Lecture Notes in Computer Science. Springer International Publishing, Oct. 2016. 3

[12] C. Lassner, J. Romero, M. Kiefel, F. Bogo, M. J. Black, and P. V. Gehler, "Unite the people: Closing the loop between 3d and 2d human representations," *CoRR*, vol. abs/1701.02468, 2017. [Online]. Available: http://arxiv.org/abs/1701.02468 3

[13] M. Loper, N. Mahmood, J. Romero, G. Pons-Moll, and M. J. Black, "Smpl: A skinned multi-person linear model," *ACM Trans. Graph.*, vol. 34, pp. 248:1–248:16, 2015. 3

[14] D. Anguelov, P. Srinivasan, D. Koller, S. Thrun, J. Rodgers, and J. Davis, "Scape: Shape completion and animation of people," *ACM Transactions on Graphics*, 2005. 3

[15] L. Pishchulin, S. Wuhrer, T. Helten, C. Theobalt, and B. Schiele, "Building statistical shape spaces for 3d human modeling," *Pattern Recognition*, vol. 67, pp. 276–286, 2017. 3

[16] N. Hasler, C. Stoll, M. Sunkel, B. Rosenhahn, and H. Seidel, "A statistical model of human pose and body shape," *Comput. Graph. Forum*, vol. 28, no. 2, pp. 337–346, 2009. [Online]. Available: https://doi.org/10.1111/j.1467-8659.2009.01373.x 3

[17] Y. Yang, Y. Yu, Y. Zhou, S. Du, J. Davis, and R. Yang, "Semantic parametric reshaping of human body models," in *2nd International Conference on 3D Vision (3DV), 2014*. Piscataway, NJ: IEEE, 2014, pp. 41–48. 3

[18] G. Varol, J. Romero, X. Martin, N. Mahmood, M. J. Black, I. Laptev, and C. Schmid, "Learning from synthetic humans," in *CVPR*, 2017. 3, 4, 6

[19] H. Joo, T. Simon, and Y. Sheikh, "Total capture: A 3d deformation model for tracking faces, hands, and bodies," *CoRR*, vol. abs/1801.01615, 2018. [Online]. Available: http://arxiv.org/abs/1801.01615 3

[20] A. A. A. Osman, T. Bolkart, and M. J. Black, "Star: Sparse trained articulated human body regressor," in *European Conference on Computer Vision (ECCV)*, Aug. 2020. 3, 4

[21] B. Allen, B. Curless, and Z. Popović, "The space of human body shapes," in *ACM SIGGRAPH 2003 Papers on - SIGGRAPH '03*, A. P. Rockwood, Ed. New York, New York, USA: ACM Press, 2003, p. 587. 3

[22] S. Wuhrer and C. Shu, "Estimating 3d human shapes from measurements," *Mach. Vis. Appl.*, vol. 24, no. 6, pp. 1133–1147, 2013. [Online]. Available: https://doi.org/10.1007/s00138-012-0472-y 3

[23] J. Boisvert, C. Shu, S. Wuhrer, and P. Xi, "Three-dimensional human shape inference from silhouettes: Reconstruction and validation," *Machine Vision and Applications*, vol. 24, no. 1, pp. 145–157, 2013. 3

[24] E. Dibra, H. Jain, C. Öztireli, R. Ziegler, and M. Gross, "Hs-nets: Estimating human body shape from silhouettes with convolutional neural networks," in *2016 Fourth International Conference on 3D Vision (3DV)*. IEEE, 2016, pp. 108–117. 3

[25] E. Dibra, A. C. Öztireli, R. Ziegler, and M. H. Gross, "Shape from selfies: Human body shape estimation using cca regression forests," in *ECCV*, 2016. 3

[26] M. Piccirilli, "Machine learning approaches to human body shape analysis," Ph.D. dissertation, 2018. [Online]. Available: https://doi.org/10.33915/etd.6417 3

[27] A. Kanazawa, M. J. Black, D. W. Jacobs, and J. Malik, "End-to-end recovery of human shape and pose," in *Computer Vision and Pattern Regognition (CVPR)*, 2018. 3

[28] J. Wang, C. Wen, Y. Fu, H. Li, T. Zou, X. Xue, and Y. Zhang, "Neural pose transfer by spatially adaptive instance normalization," in *Proceedings of the IEEE/CVF Conference on Computer Vision and Pattern Recognition*, 2020, pp. 5831–5839. 3

[29] T. Alldieck, G. Pons-Moll, C. Theobalt, and M. Magnor, "Tex2shape: Detailed full human body geometry from a single image," in *IEEE International Conference on Computer Vision (ICCV)*, 2019. 3

[30] S. Li, L. Ke, K. Pratama, Y.-W. Tai, C.-K. Tang, and K.-T. Cheng, "Cascaded deep monocular 3d human pose estimation with evolutionary training data," in *The IEEE/CVF Conference on Computer Vision and Pattern Recognition (CVPR)*, June 2020. 3

[31] N. Kolotouros, G. Pavlakos, and K. Daniilidis, "Convolutional mesh regression for single-image human shape reconstruction," in *CVPR*, 2019. 3

[32] G. Varol, D. Ceylan, B. Russell, J. Yang, E. Yumer, I. Laptev, and C. Schmid, "BodyNet: Volumetric inference of 3D human body shapes," in *ECCV*, 2018. 3

[33] V. Choutas, G. Pavlakos, T. Bolkart, D. Tzionas, and M. J. Black, "Monocular expressive body regression through body-driven attention," in *European Conference on Computer Vision (ECCV)*, 2020. [Online]. Available: https://expose.is.tue.mpg.de 3

[34] B. M. Auerbach and C. B. Ruff, "Limb bone bilateral asymmetry: variability and commonality among modern humans," *Journal of Human Evolution*, vol. 50, no. 2, pp. 203–218, 2006. [Online]. Available: https://www.sciencedirect.com/science/article/pii/S004724840500165X 5

[35] B. O. Community, "Blender - a 3d modelling and rendering package." [Online]. Available: https://github.com/blender/blender 6

[36] A. Paszke, S. Gross, F. Massa, A. Lerer, J. Bradbury, G. Chanan, T. Killeen, Z. Lin, N. Gimelshein, L. Antiga, A. Desmaison, A. Kopf, E. Yang, Z. DeVito, M. Raison, A. Tejani, S. Chilamkurthy, B. Steiner, L. Fang, J. Bai, and S. Chintala, "Pytorch: An imperative style, high-performance deep learning library," in *Advances in Neural Information Processing Systems 32*, H. Wallach, H. Larochelle, A. Beygelzimer, F. d'Alché-Buc, E. Fox, and R. Garnett, Eds. Curran Associates, Inc., 2019, pp. 8024–8035. [Online]. Available: http://papers.neurips.cc/paper/9015-pytorch-an-imperative-style-high-performance-deep 6

[37] V. Nair and G. E. Hinton, "Rectified linear units improve restricted boltzmann machines," in *Proceedings of the 27th International Conference on International Conference on Machine Learning*, ser. ICML'10. Madison, WI, USA: Omnipress, 2010, p. 807–814. 6

[38] I. Sutskever, J. Martens, G. E. Dahl, and G. E. Hinton, "On the importance of initialization and momentum in deep learning," in *Proceedings of the 30th International Conference on Machine Learning, ICML 2013, Atlanta, GA, USA, 16-21 June 2013*, ser. JMLR Workshop and Conference Proceedings, vol. 28. JMLR.org, 2013, pp. 1139–1147. [Online]. Available: http://proceedings.mlr.press/v28/sutskever13.html 6